RSC Advances

ROYAL SOCIETY OF CHEMISTRY

www.rsc.org/advances

Cite this: DOI: 10.1039/c0xx00000x

www.rsc.org/xxxxxx

ARTICLE TYPE

Facile fabrication of 3D flower-like heterostructured g-C_3N_4/SnS_2 composite with efficient photocatalytic activity under visible light

Meng Sun,[a] Qing Yan,[a] Tao Yan,[b,c] Mengmeng Li,[b] Dong Wei,[a] Zhongpeng Wang,[a] Qin Wei,[d] and Bin Du*[a]

Received (in XXX, XXX) XthXXXXXXXXX 20XX, Accepted Xth XXXXXXXXX 20XX
DOI: 10.1039/b000000x

Abstract: 3D flower-like heterostructured g-C_3N_4/SnS_2 composites were fabricated by a facile solvothermal method. The obtained g-C_3N_4/SnS_2 composites were characterized by X-ray diffraction (XRD), scanning electron microscopy (SEM), high-resolution transmission electron microscopy (HRTEM), N_2 sorption–desorption, and ultraviolet-visible diffuse reflection spectroscopy (DRS). The SEM results showed that the SnS_2 nanoflakes assembled into hierarchical flowers when g-C_3N_4 was introduced into the system. The elemental mapping images revealed that g-C_3N_4 and SnS_2 nanoflakes uniformly assembled together to form the hierarchical flowers. The HRTEM image showed clear heterojunction structure at the interfaces between g-C_3N_4 and SnS_2 nanoflakes. The DRS characterization showed that the light absorption exhibited regular red-shifts upon the increasing of g-C_3N_4/SnS_2 mass ratio. In the photocatalytic reduction of aqueous Cr(VI) under visible-light irradiation, g-C_3N_4/SnS_2 composites exhibited enhanced activities, which were greatly higher than that for pure SnS_2, SnS_2/TiO_2, and PM-g-C_3N_4/SnS_2 (A physical mixture of g-C_3N_4 and SnS_2). The photoelectrochemical measurement confirmed that the separation efficiency of electron–hole pairs was greatly improved for the formation of heterojunction structure. It was also shown that the formate or hydrogen ions added systematically accelerated the photo-reduction rates of Cr(VI). A possible photocatalytic mechanism for g-C_3N_4/SnS_2 composites was proposed.

Keywords: g-C_3N_4/SnS_2; 3D flower-like; Photocatalysis; Visible light; Cr(VI) reduction

Introduction

The aquatic environmental imbalance mainly occurs because of the contamination of water with harmful materials. Unlike organic pollutants, the heavy metal ions are particularly problematic because they are not biodegradable but can be accumulated in living tissues. Thus, the metal ions are becoming concentrated throughout the food chain, and a slightly higher dose could severely endanger the health of most living organisms.[1] Cr(VI) is a common pollutant in the wastewater discharged from leather tanning, electroplating, mining and chromate manufacturing, etc. Because of the carcinogenicity and mutagenicity, Cr(VI) has been included in the list of priority pollutants and its maximum concentrations in drinking water and discharged industrial wastewaters have been regulated by many countries.[2-4] Therefore, it is very important for us to find a new way to treat Cr(VI) efficiently and economically in wastewater.

The strategy based on Cr(VI) reduction and consequent precipitation has been used for Cr(VI) removal because Cr(III) exhibits a lower toxicity and mobility in the environment. However, the conventional chemical reduction methods usually need great quantities of reductant, such as ferrous sulfate or sulfur dioxide, which is consumed and difficult to be recycled. In addition, the residual reductant and bases added in the following precipitation process of Cr(III) always result in secondary environmental pollution.[5] On the contrary, the semiconductor-mediated photocatalytic reduction technology as a new method for treating aqueous Cr(VI) has some obvious advantages, such as simple operation, ambient conditions, low cost, high efficiency, and no use or release of other unwanted chemicals.[6-12] Consequently, the photocatalytic reduction method has been widely regarded as a promising way for the removal of Cr(VI).

The exploitation of highly active photocatalyst is vital for photocatalysis technique to be used in treating Cr(VI)-contaminated wastewater. TiO_2 has been widely studied as a semiconductor photocatalyst for decomposing organic pollutants.[13-16] The photocatalytic reduction of Cr(VI) over TiO_2 has also been reported. In our previous study, $CaSb_2O_5(OH)_2$ has

[a]*School of Resources and Environment, University of Jinan, Shandong Provincial Engineering Technology Research Center for Ecological Carbon Sink and Capture Utilization, Jinan250022, P.R. China. Fax: +86 531-82765969; Tel:+86 531-82769235;E-mail:binduujn@163.com*
[b]*School of Civil Engineering and Architecture, University of Jinan, Jinan250022, P.R. China.*
[c]*School of Chemistry, Beijing Institute of Technology, Beijing 100081, P.R. China*
[d]*Key Laboratory of Chemical Sensing & Analysis in Universities of Shandong, School of Chemistry and Chemical Engineering, University of Jinan, Jinan 250022, P.R. China*

been found more photo-active than TiO_2 in the reduction of Cr(VI) under UV light illumination.[17] However, due to their wide band gaps, TiO_2 and $CaSb_2O_5(OH)_2$ can not be activated by visible light, which accounts for about 46% of the total solar energy.[18] In order to make full use of solar energy, it is desirable to develop new visible light-responsive photocatalysts. Zhuang et al. have reported the preparation of SnO_2-graphene aerosol with excellent visible light photocatalytic activity toward organic pollutants.[19] Pd nanoparticle-immobilized electrospun polymer nanofibers and TiO_2/CdS nanocomposite have also been reported as visible light-responsive photocatalysts for catalytic reduction of Cr(VI) to Cr(III).[20,21]

Recently, Zhang et al. have reported the photo-reduction of Cr(VI) over SnS_2, which is commonly used a visible light-responsive photocatalyst.[22-24] The conduction band potential of SnS_2 is about –0.114 V (vs. NHE).[25] In order to further improve the activity for Cr(VI) reduction, SnS_2 has been used to combine with TiO_2, but the activity of SnS_2/TiO_2 (SSTI) composite is still not satisfactory.[26]

Polymeric graphitic carbon nitride (g-C_3N_4) as a metal-free polymeric photocatalyst has been reported by Wang et al. It is a very promising material for solar energy utilization because of its high thermal and chemical stability, semi-conductivity, and desirable band gap of 2.7 eV.[27,28] Moreover, the g-C_3N_4 is inexpensive and its synthesis process is comparatively simple, rendering g-C_3N_4 attracts a great deal of scientific interest, specially its applications in photo-splitting of water.[29-32] and degradation of organic pollutants.[33-36] We have found that the conduction band potential of g-C_3N_4 (–1.3 V vs NHE) is more negative than the reduction potential of Cr(VI)/Cr(III) (1.23 V), it is possible for g-C_3N_4 to reduce Cr(VI) under visible light thermodynamically.[37] Unfortunately, pure g-C_3N_4 suffers from poor photo-reactivity resulted from the low charge separation efficiency. Herein, we first use g-C_3N_4 to combine with SnS_2 to improve the separation efficiency of photo-generated electron-hole pairs. And the experiment results shows that through the combination of g-C_3N_4 and SnS_2, the as-synthesized g-C_3N_4/SnS_2 composites have exhibited excellent activities higher than that of pure SnS_2, g-C_3N_4, SSTI, and the physical mixture of g-C_3N_4/SnS_2 under visible light (800 nm > λ > 420 nm) irradiation.

Experimental section

Synthesis of g-C_3N_4

All the reagents were analytical-grade and used as received without further purification. The g-C_3N_4 sample was first synthesized by heating melamine in a muffle furnace according to the literatures with small modification.[38,39] In a typical experiment, 5.0 g of melamine was put into a semi-closed alumina crucible with a cover, which was then placed in a muffle furnace and heated to 550 °C at a heating rate of 5 °C min^{-1}. After 4 h of reaction, the alumina crucible was cooled to room temperature, and the products were collected and ground into powders.

Synthesis of 3D flower-like g-C_3N_4/SnS_2 composites

In synthesizing g-C_3N_4/SnS_2 composites, 5.0 mmol $SnCl_4 \cdot 5H_2O$ was added into a 50 mL Teflon-lined stainless steel autoclave. And then, 2.0 mL of acetic acid and 38.0 mL of ethanol were mixed together and added into the above solution with stirring. After the dissolution of $SnCl_4 \cdot 5H_2O$, an appropriate amount of g-C_3N_4 was added and ultrasonicated for 15 min to completely disperse the g-C_3N_4. Then, 10.0 mmol thioacetamide was added and stirred for 5 h at room temperature. The autoclaves were sealed and heated in an electric oven at 180 °C for 12 h, and then cooled to ambient temperature naturally. The resultant precipitates were filtered, washed with deionized water, and dried in vacuum at 80 °C for 4 h. Pure SnS_2 powders were fabricated through a similar procedure in the absence of g-C_3N_4.

According to this method, g-C_3N_4/SnS_2 composites with different mass ratios of 20%, 30%, 40%, and 50% were synthesized and named as CNSS-20, CNSS-30, CNSS-40, and CNSS-50, respectively. PM-CNSS-30 is the abbreviation for the g-C_3N_4/SnS_2 composite prepared by physical mixing method with the same composition as CNSS-30 (30 wt% g-C_3N_4 and 70 wt% SnS_2 powders physical mixed without any treatment). The SSTI (44.5 mass% TiO_2) composite photocatalyst was synthesized according to the literature as a comparison.[26]

Characterization of photocatalysts

The crystallographic phase of these obtained products was determined by powder X-ray diffraction (XRD; Bruker D8 Advance, Cu Kα radiation). The morphologies and microstructures of the samples were observed by a Hitachi S-4800 scanning electron microscopy (SEM) and a JEOL model JEM 2010 EX high-resolution transmission electron microscopy (HRTEM). Nitrogen sorption experiment was carried out at 77 K by using Micromeritics ASAP2020 equipment. The diffuse reflectance ultraviolet–visible light spectra (DRS) were recorded with a UV–vis spectrophotometer (Cary 500 Scan Spectrophotometers, Varian, and U.S.A) equipped with an integrating sphere attachment at room temperature and transformed to the absorption spectrum according to the Kubelka-Munk relationship.

Photocatalytic tests

Photocatalytic reactions were conducted in a customized reactor with a cooling-water-cycle system keeping the temperature of the aqueous solution was maintained at 25 ºC. The visible light photocatalytic activities of g-C_3N_4/SnS_2 composites were evaluated by the photocatalytic reduction of aqueous Cr(VI) using a 300 W xenon lamp (Beijing Perfect Light Co. Ltd., Beijing) with a cutoff filter (λ > 420 nm) as light source. In each experiment, 40 mg of photocatalyst was dispersed into 100 mL of $K_2Cr_2O_7$ (50 mg/L) aqueous solution. Before irradiation, the suspensions were magnetically stirred in dark for 60 min to ensure the establishment of an adsorption/desorption equilibrium between the photocatalyst and Cr(VI). During the reaction under visible light irradiation, 3.0 mL of suspension was sampled at given time intervals and centrifuged to remove the photocatalyst. The Cr(VI) contents in the supernatant solutions were determined colorimetrically at 540 nm using the standard diphenylcarbazide method with a detection limit of 5 μg/L. The measured absorbance intensities at different illumination times were transformed to the reduction ratio of Cr(VI), which can be defined as the following expression:

$$\text{Reduction ratio of Cr(VI)} = (C_0 - C_t)/C_0 \times 100\%$$

where C_0 and C_t are the absorbance intensities when illuminated for 0 and t min, respectively.

Photocurrent measurements (PC)

The photocurrent measurements were conducted on CHI 760E electrochemical workstation (CHI 760E Chenhua Instrument Company, Shanghai, China) in a conventional three-electrode configuration with a Pt wire as the counter electrode and a saturated calomel electrode as reference electrode. Irradiation proceeded by a Xe arc lamp through a UV cut off filter ($\lambda > 420$ nm). Na_2SO_4 (1.0 M) aqueous solution was used as the electrolyte. The working electrodes were prepared as follows: An indium tin oxide (ITO) glass piece with a size of 2.0 × 1.0 cm was cleaned successively by acetone, ethanol, deionized water, and then dried in an air stream. 3.0 mg of the ground sample was dispersed uniformly with 1.0 mL of distilled water under the condition of ultrasonic, and 10 μL of above solution was added to surface of the ITO and dried at 120 °C for 30 min. This prepared working electrode was used as the photocathode, and the current polarity was cathodic positive in the system setup.

Electrochemical impedance spectroscopy (EIS)

EIS measurements were performed in 2.5 mM $K_3Fe(CN)_6/K_4Fe(CN)_6$ (1:1) containing 0.1 M KCl with a frequency range from 0. 1 Hz to 100 kHz at 0.24 V, and the amplitude of the applied sine wave potential in each case was 5 mV. A modified glassy carbon electrode (GCE, 4 mm diameter) as the working electrode, which was prepared by a simple method as follows: g-C_3N_4 homogeneous suspension was prepared by dispersing 5 mg g-C_3N_4 in 1 mL distilled water. Then, 20 μL of the slurry was dripped on the GCE and dried at 60 °C for 120 min (denoted as CN/GCE). SS/GCE and CNSS-30/GCE with the same quantity was prepared using the same procedure.

Results and discussion

Structural characterization

Figure 1 shows the XRD patterns of the as-prepared g-C_3N_4, SnS_2, and g-C_3N_4/SnS_2 composites with different mass ratios. As we can see, the pure g-C_3N_4 sample is with two distinctive diffraction peaks located at 27.4° and 13.1°, which are indexed to the (002) and (100) diffraction planes of g-C_3N_4, respectively (JCPDS 87-1526). The typical XRD patterns for pure SnS_2 are shown in Figure 1g. And all the diffraction patterns are well matched with the hexagonal SnS_2 (JCPDPS 22-0951) with a lattice constant a=3.649 Å and c=5.899 Å. The observed XRD results are well matched with already reported literature. The XRD patterns of g-C_3N_4/SnS_2 composites with various contents of g-C_3N_4 are shown in Figure 1b-f. It has been found that the peaks intensities of SnS_2 have become relatively weaker with the increase of g-C_3N_4 content. In addition, due to the superposition of the peak for SnS_2 (28.4°) and g-C_3N_4 (27.4°), the peak located at 28.4° for g-C_3N_4/SnS_2 composites becomes broader than that for pure SnS_2. Moreover, no impurity phase has been observed, indicating that the synthesized composite presents a two-phase composition.

The general morphologies of as-prepared g-C_3N_4, SnS_2, and g-C_3N_4/SnS_2 have been examined by SEM. Figure 2a shows the morphology of the as-prepared g-C_3N_4, where irregular larger particles and sheets are observed. As shown in Figure 2b, the obtained SnS_2 exhibits nanoflake morphology and the flakes

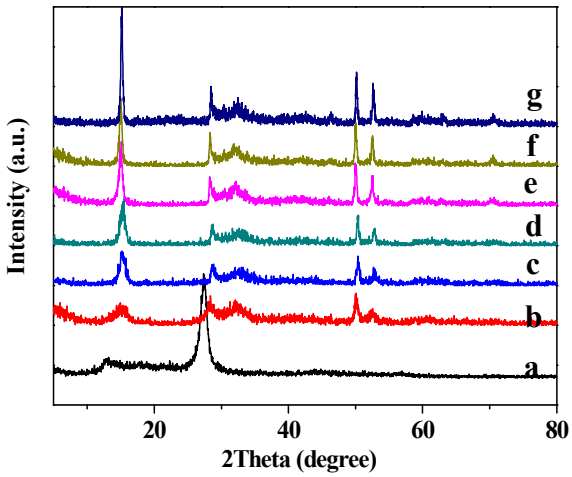

Figure 1. XRD patterns of g-C_3N_4/SnS_2 composites with different g-C_3N_4 contents: (a) pure g-C_3N_4, (b) CNSS-50, (c) CNSS-40, (d) CNSS-30, (e) CNSS-20, (f) CNSS-10, and (g) pure SnS_2.

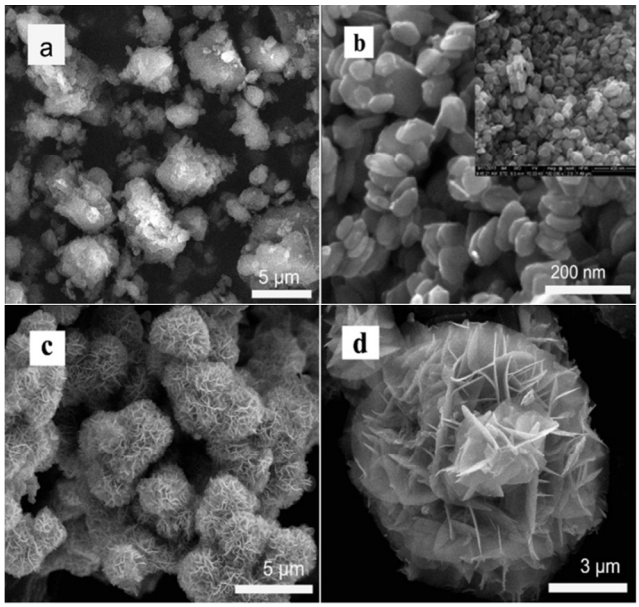

Figure 2. SEM images of (a) pure g-C_3N_4, (b) pure SnS_2, and (c)-(d) CNSS-30 sample.

are randomly arranged. However, when a certain amount of g-C_3N_4 was introduced to combine with SnS_2, the obtained g-C_3N_4/SnS_2 composites exhibited a perfect 3D flower-like nanostructure with well-arranged nanoflakes on the surfaces (shown in Figure 2c-d). The formation of this flowerlike morphology might be ascribed to the self-assembly of SnS_2 nanoflakes. The g-C_3N_4 sheets added in the reaction solutions might affect the nucleation and crystal growth processes of SnS_2 under the solvothermal condition. Figure 2c-d shows that the as-synthesized g-C_3N_4/SnS_2 flowers possess an average diameter of 3–5 μm, which are mainly constructed by SnS_2 nanoflakes. The SnS_2 nanoflakes connected to each other to form 3D flowerlike structures. Because g-C_3N_4 was prior added in the reaction solution, when SnS_2 crystallized to form nanoflakes and nanoflowers, g-C_3N_4 sheets would also be entangled in the hierarchical structure. And thus, g-C_3N_4 and SnS_2 would

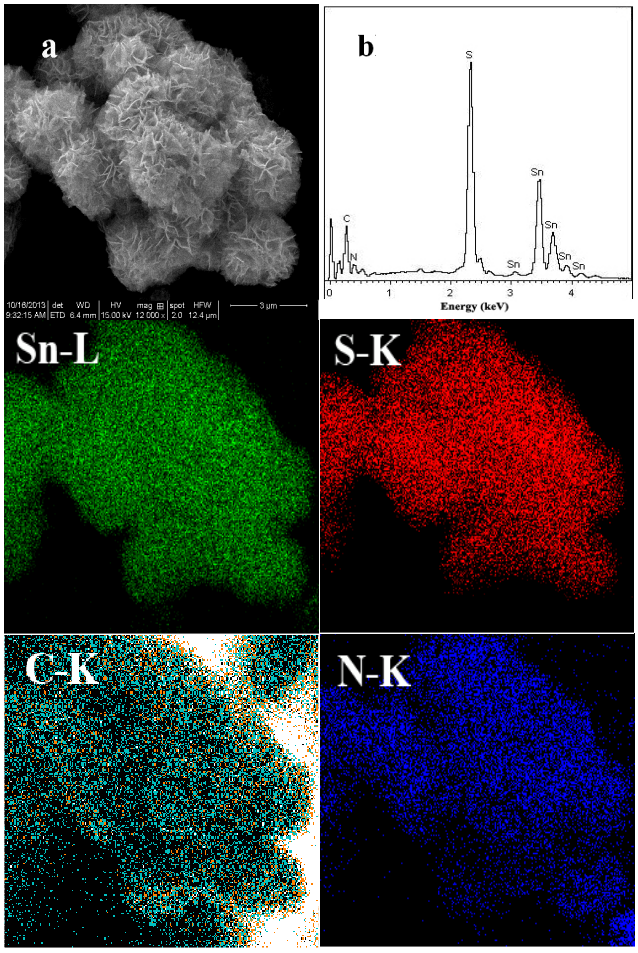

Figure 3. The SEM image (a) and EDS spectrum (b) of CNSS-30 sample and corresponding elemental mapping images of Sn, S, C, and N elements.

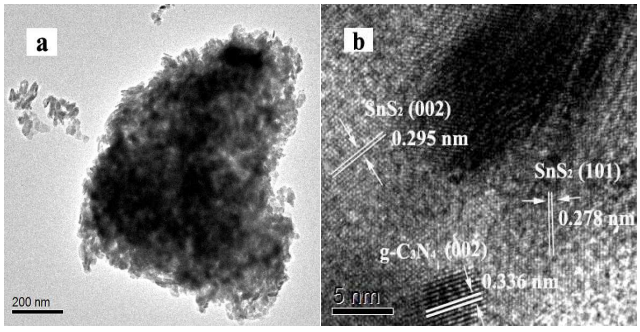

Figure 4. TEM and HRTEM images of the as-prepared sample. (a) TEM micrographs of g-C_3N_4/SnS_2 composites. (b) HRTEM image of g-C_3N_4/SnS_2 composites showing the formation of heterojunction structure.

homogeneous combined together to form heterojunction at their interfaces, which was beneficial for improving the separation ratio of photo-generated electron-hole pairs.

The elemental mapping has been conducted to investigate the distribution of g-C_3N_4 in the g-C_3N_4/SnS_2 composites. Figure 3 displays the elemental mapping images for the sample. The red, black, and blue color of the image was respectively acquired at the K-line spectra of S, C, and N elements, while that for the green color was acquired at the L-line spectra of Sn element. It can be seen that the elements of C and N have a homogenous distribution in the SnS_2 hierarchical nanoflowers. This provides solid evidence that SnS_2 nanoflowers were successfully combined with g-C_3N_4. Figure 4 shows the microstructures of the g-C_3N_4/SnS_2 composites via TEM and HRTEM. As we can see, one fringe with d = 0.336 nm matches the (002) crystallographic plane of g-C_3N_4. The lattice spaces of the SnS_2 crystallites were determined as 0.278 and 0.295 nm, belonging to the (101) and (002) crystallographic planes of hexagonal SnS_2. Figure 4b shows that after solvothermal treatment, obvious interface between g-C_3N_4 and SnS_2 nanoflakes can be observed. This finding suggests that the heterojunction structure is indeed formed at the interfaces of those two materials.

DRS and BETcharacterization

The UV-vis diffuse reflectance spectra of g-C_3N_4, SnS_2, and g-C_3N_4/SnS_2 composites were investigated using a UV–vis spectrometer. Compared with pure g-C_3N_4 and SnS_2, the absorption edges of the g-C_3N_4/SnS_2 composites are slightly red-shifted. Based on the Kubelka–Munk equation, the band gap of the two semiconductors can be deduced.[40] g-C_3N_4 has a band gap of 2.70 eV, while SnS_2 has a band gap of about 2.10 eV. Shanker et al. have reported that the slightly red shift might suggest that the recombination rate of the electron–hole pair was successfully reduced.[41] The BET surface areas of the samples are shown in Table 1. As we can see, the SnS_2 nanoflakes possess a relatively large surface area of 65.3 m^2/g. For the g-C_3N_4/SnS_2 composites, the surface area decreases with the enhancement of g-C_3N_4 mass ratio because the surface area of g-C_3N_4 is only 7.5 m^2/g. The following degradation experiment shows that the change in the surface area did not match that in the catalyst activity. Therefore, the most important factor that influenced the catalytic activity might be the catalyst composition but not the surface area.

Table 1 S_{BET} values and photocatalytic activities of g-C_3N_4/SnS_2 composites.

Name	S_{BET} (m^2/g)	Reaction rate constant k ($mol^{-1} \cdot dm^3 \cdot min^{-1}$)	R^2
SnS_2	65.3	0.0482	0.96
CNSS-20	51.4	0.0746	0.96
CNSS-30	46.8	0.4582	0.99
CNSS-40	37.7	0.3742	0.99
CNSS-50	30.1	0.1869	0.98
g-C_3N_4	7.5	0.0003	-

Photocatalytic reduction of aqueous Cr(VI)

To investigate the effect of g-C_3N_4 content on the photocatalytic activity of g-C_3N_4/SnS_2 composites, g-C_3N_4/SnS_2 composites with different mass ratios have been used in the photocatalytic reduction of aqueous Cr(VI) under the same conditions. Figure 6 shows the visible light photocatalytic activities of the as-synthesized SnS_2, g-C_3N_4/SnS_2 composites, and g-C_3N_4 in the reduction of aqueous Cr(VI). As it can be seen, the activity of g-C_3N_4/SnS_2 composite was much higher than that for SnS_2 and g-C_3N_4. The g-C_3N_4 content has great influences on the photocatalytic activity. After 50 min of visible light irradiation, the reduction ratio of Cr(VI) over SnS_2 and g-C_3N_4 was 71.8 and 3.1 %, respectively. As for the g-C_3N_4/SnS_2 composites, when

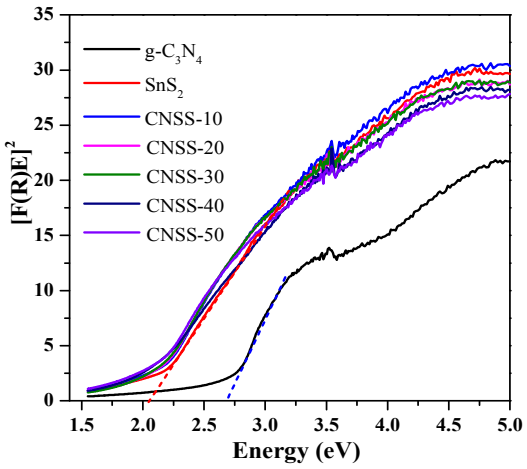

Figure 5. UV–vis spectra of g-C_3N_4/SnS_2 composites with different g-C_3N_4 concentration and estimated band gap of photocatalyst by Kubelka Munk function.

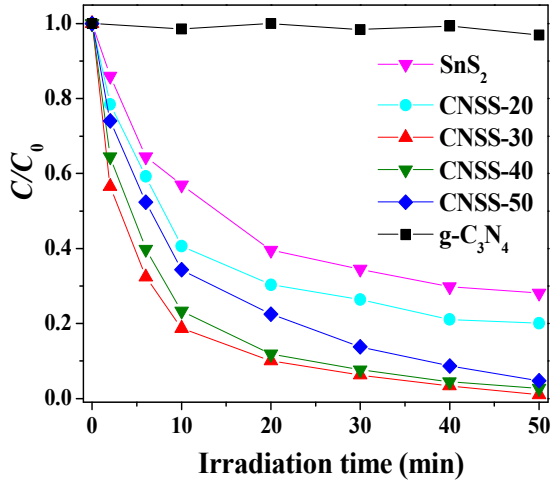

Figure 6. Photocatalytic reduction curves of aqueous Cr(VI) over pure g-C_3N_4, SnS_2, and g-C_3N_4/SnS_2 composites under visible light irradiation.

the g-C_3N_4 content changed from 20 to 30 wt.%, the photocatalytic reduction rates of Cr(VI) were greatly improved, and about 99% of Cr(VI) has been deoxidized within 50 min of reaction. However, when the g-C_3N_4 content further increased from 30 to 50 wt.%, the photocatalytic activity of g-C_3N_4/SnS_2 composites gradually decreased. The excellent photocatalytic activity of CNSS-30 composite should be ascribed to its high charge separation efficiency, and this has also been further proved by the following EIS and photocurrent measurements. Figure S1 shows that the absorption intensity of DPC-Cr(VI) complex gradually decreased with the increase of irradiation time in the presence of CNSS-30 composite. After 50 min of irradiation, the absorption peak of DPC-Cr(VI) complex almost disappeared. It has also been found that the photocatalytic reduction of Cr(VI) followed the second-order kinetics (Figure S2), and the kinetic constant (k) were shown in Table 1.

To evaluate the photocatalytic activities of g-C_3N_4/SnS_2 composites, the recently reported visible light photocatalyst SnS_2/TiO_2 was also prepared as a comparison.[26] Figure 7 shows the photocatalytic reduction of Cr(VI) over g-C_3N_4/SnS_2, SnS_2/TiO_2, and PM-g-C_3N_4/SnS_2 composites under visible light illumination. As we can see, with absence of any photocatalyst the reduction of Cr(VI) hardly occurred when subjected to visible light irradiation. In contrast, after 10 min of visible light irradiation, the reduction ratio of aqueous Cr(VI) over SnS_2/TiO_2 was about 53.2%, while that for CNSS-30 was 81.3%, which was further increased to 99% after 50 min of continuous reaction. Remarkably, the photocatalytic activity of CNSS-30 was greatly higher than that for SnS_2/TiO_2 composite.

To prove the activity enhancement was mainly ascribed to the formation of heterojunction at the interface of g-C_3N_4 and SnS_2, a controlled experiment has been done. A physical mixture of g-C_3N_4 and SnS_2 (PM-g-C_3N_4/SnS_2) has also been used to photocatalytic deoxidize aqueous Cr(VI) as a comparison. Without solvothermal treatment, the formation of heterojunction structure becomes impossible in PM-g-C_3N_4/SnS_2. The reduction ability of this PM-g-C_3N_4/SnS_2 composite was shown in Figure 7. It can be clearly seen that the photocatalytic performance of CNSS-30 was obviously higher than that of PM-g-C_3N_4/SnS_2. After 50 min of visible light irradiation, the reduction of aqueous Cr(VI) over CNSS-30 was up to 99.1%, while that over PM-g-C_3N_4/SnS_2 was only 56.1%. Therefore, the formation of heterojunction structure in solvothermal treatment results in the faster charge transfer rate and higher separation ratio of electron-hole pairs.

Figure 8 shows the reduction evolution of aqueous Cr(VI) at different dosages of CNSS-30 photocatalyst under visible light irradiation. It is evident that the reduction rates of aqueous Cr(VI) has been generally improved when the amount of CNSS-30 used was increased from 0.02 to 0.08 g, and nearly 100% of aqueous Cr(VI) had been photocatalytic deoxidized within 20 min of visible light irradiation. The enhancement of reduction rates with increased photocatalyst concentrations is a characteristic of heterogeneous catalysis, and it can be rationalized in terms of the availability of active cites on the photocatalyst surface as well as the light penetration into the suspensions. In addition, Figure 8 also shows that without visible light irradiation, the reduction of

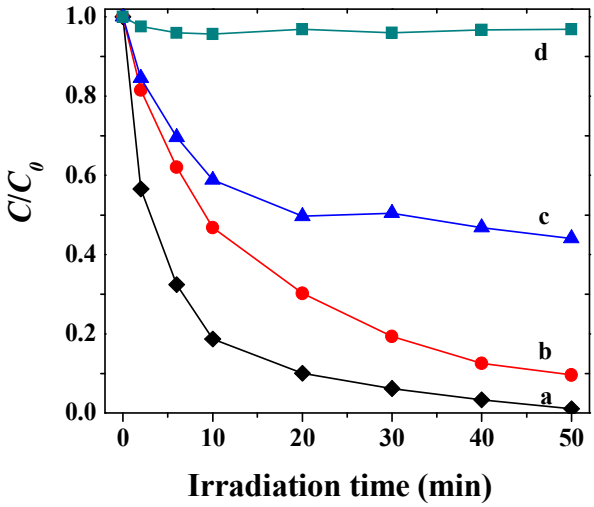

Figure 7. Comparisons of photocatalytic reduction of aqueous Cr(VI) on (a) CNSS-30, (b) SSTI, (c) PM-CNSS-30, and (d) no catalyst under visible light ($\lambda > 420$ nm) irradiation.

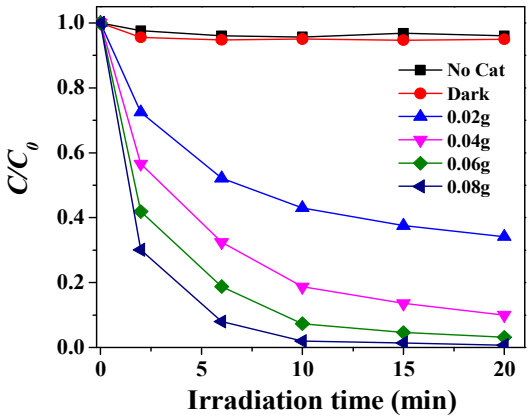

Figure 8. Photocatalytic reduction of Cr(VI) with different dosages of CNSS-30 under the visible light (λ > 420 nm) irradiation.

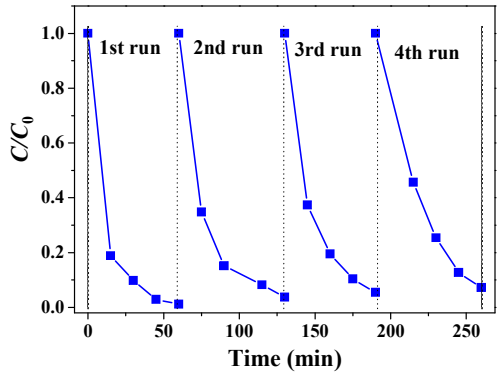

Figure 9. Photocatalytic performances of CNSS-30 composite photocatalyst in the first four reuse cycles.

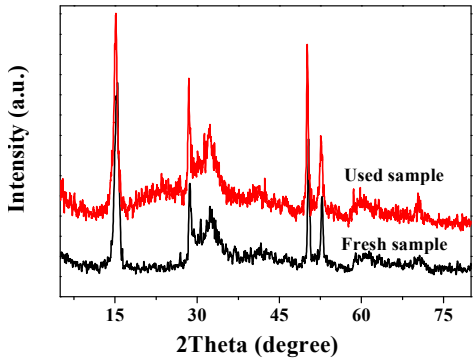

Figure 10. XRD patterns of CNSS-30 before and after photocatalytic reduction of Cr(VI).

Cr(VI) can hardly occur over CNSS-30 composite. Thus, it is inferred that the removal of aqueous Cr(VI) is dominatingly a photocatalytic reduction process, but not just simple physical adsorption.

The g-C_3N_4/SnS_2 composite not only exhibited efficient photocatalytic activities, but also revealed good stability in the Cr(VI) reduction process. In the current work, g-C_3N_4/SnS_2 composite was recycled for four times in the same photocatalytic reactions. And the life-time test results were shown in Figure 9. It shows that the photocatalytic activity of g-C_3N_4/SnS_2 composite only deteriorated slightly in the reuse cycles. Figure 10 shows the XRD patterns of g-C_3N_4/SnS_2 composites before and after Cr(VI) reduction. It illustrates that the crystal structure of the g-C_3N_4/SnS_2 photocatalyst was not changed during the reaction.

Separation efficiency of photo-generated electron-hole pairs

The generation and separation of photo-generated electron-hole pairs is very important for the enhancement of photocatalytic activity. In this study, photocurrent and EIS have been used to investigate the interfacial charge separation efficiency over different photocatalysts. As it can be seen from Figure 11, the diameter of the Nyquist circle of CNSS-30 composite is smaller than that of pure SnS_2, g-C_3N_4, and other g-C_3N_4/SnS_2 composites, indicating that the CNSS-30 composite has a relatively lower resistance compared with other samples. That is to say, the introduction of g-C_3N_4 into SnS_2 could enhance the separation efficiency and transfer rate of photo-generated carriers,[42] which is favorable for enhancing the photocatalytic activity.

Figure 12 shows the results of photocurrent measurements that carried out at open circuit potentials under visible light illumination. As we can see, fast and uniform photocurrent responses have been observed in all electrodes. But the photocurrent density observed over CNSS-30 composite was higher than that produced over pure SnS_2, g-C_3N_4, SSTI, and other g-C_3N_4/SnS_2 composites, indicating that the photo-generated electron/hole pairs were separated more efficiently over CNSS-30 composite under visible light irradiation. This may explain why CNSS-30 composite exhibited the most efficient activity compared with other samples (see Figure 7).

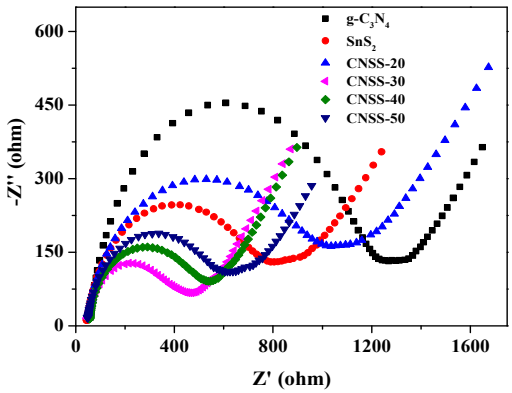

Figure 11. EIS profiles of pure g-C_3N_4, SnS_2, and g-C_3N_4/SnS_2 composites

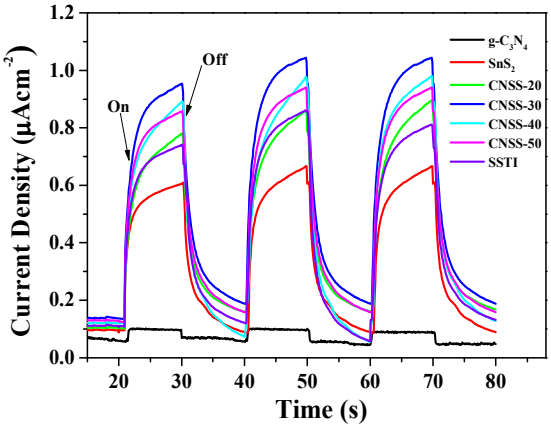

Figure 12. Transient photocurrent response for pure g-C_3N_4, SnS_2, SSTI, and g-C_3N_4/SnS_2 composites.

Effect of pH on Cr(VI) photocatalytic reduction

Ku et al. reported the photocatalytic reduction rates of aqueous Cr(VI) could be greatly accelerated in acidic solutions.[43] In order to study the influences of pH on the reduction of Cr(VI), controlled experiments have been done with H_2SO_4 solution (1.0 M) added. Figure 13 shows the photocatalytic reduction of Cr(VI) over CNSS-30 with different amounts of 1.0 M H_2SO_4 added. As we can see, when 0.5 mL of 1.0 M H_2SO_4 was added, the reduction ratio of Cr(VI) was increased from 81 to 98% within 10 min reaction. When more amount of H_2SO_4 solution was added, the reduction rate could be further accelerated.

Effect of hole scavenger on Cr(VI) photocatalytic reduction

It has been reported that sacrificial reagents were helpful for enhancing the reduction rates of Cr(VI). For example, formic acid as effective sacrificial electron donor has been used as hole scavenger to improve the photocatalytic activity.[44-47] In this paper, we have mainly investigated the effects of formic acid on the reduction rates of Cr(VI) over CNSS-30 composites. Figure 14 shows the visible light photocatalytic reduction of aqueous Cr(VI) in the absence/presence of formic acid. As it can be seen, the reduction rates of Cr(VI) were greatly accelerated when increasing the amount of formic acid added. With the absence of formic acid, the reduction ratio of Cr(VI) in the first 5 min of reaction was only 70%. However, when 0.08, 0.24, and 0.38 mL of formic acid was added, the reduction ratio was respectively increased to 80, 95, and 98%. When the amounts of formic acid added increased to 0.52 mL, the Cr(VI) reduction ratio had been improved to nearly 100%. These results proves that formic acid added in the system could effectively accelerate the Cr(VI) reduction rate through depleting the photo-generated holes.

The energy band diagrams for the prepared catalysts has been presented in Scheme 1, which could help to explain why g-C_3N_4/SnS_2 exhibited distinctly reduction activities under visible light irradiation. First, the CB edges of pure g-C_3N_4 and SnS_2 are lower than the reduction potential of Cr(VI), promising the occurrence of reduction reactions. When formic acid was added in the system, the rates of Cr(VI) reduction over g-C_3N_4/SnS_2 composite would be greatly accelerated. That is to say, the photo-generated holes over the VB of g-C_3N_4/SnS_2 composite has stronger oxidization ability, which could oxidize HCOOH efficiently, and the consumption of holes could promote the separation efficiency of photo-generated carriers, leaving more electrons to deoxidize Cr(VI) in the system.

Possible photocatalytic mechanism

The efficient activity of 3D flower-like g-C_3N_4/SnS_2 composites should be ascribed to many reasons, such as enhanced separation efficiency of photo-generated carriers, matching conduction and valance band positions of materials, and the formation of heterostructures. First, the prepared SnS_2 is *p*-block metal sulfide, which contains a central metal ion with d^{10} electronic configuration.[46] Second, the proper conduction and valance band positions of g-C_3N_4 and SnS_2 sample. It is generally accepted that the migration direction of the photo-generated charge carriers depends on the relative band edge position of the two components in composite photocatalysts. Then the carriers could transfer to the catalyst surface to react with the adsorbed reactants.[48] According to the band gap structure of g-C_3N_4/SnS_2 and the effects of scavengers, a possible pathway for the photocatalytic activity enhancement mechanism of g-C_3N_4/SnS_2 photocatalyst was proposed as follows (Scheme 1): When p-n junction was formed over p-g-C_3N_4/n-SnS_2 photocatalyst, the CB and VB positions of g-C_3N_4 and SnS_2 changed to reach equilibration of Fermi levels (E_f) of g-C_3N_4 and SnS_2. Finally, the energy bands of SnS_2 shifted downward along with the Fermi level, whereas those of g-C_3N_4 shifted upward in this process. The newly formed energy band structure became to the interactive structure. Under visible-light (λ> 420 nm) illumination, g-C_3N_4 and SnS_2 could be double-excited and electron-hole pairs would be generated. With the effect of the inner electron field, the photo-induced electrons moved to the positive field (n-type SnS_2), and then reacted with Cr(VI) adsorbed on the surface of g-C_3N_4/SnS_2. At the same time, the photo-induced holes flew into the negative field (p-type g-C_3N_4) and directly react with the hole scavengers. However, when no extra reducing agents or hole scavengers were added in the system, it was generally supposed that the holes oxidized water to produce H^+ and O_2.[24,49-51] In such a way, the photo-generated electron-hole pairs would be separated effectively by p-n junction formed over the p-g-C_3N_4/n-SnS_2 composite photocatalyst. Therefore, the g-C_3N_4/SnS_2 composite had exhibited better photocatalytic properties than single g-C_3N_4 and SnS_2 in the reduction of Cr(VI) under visible light irradiation.

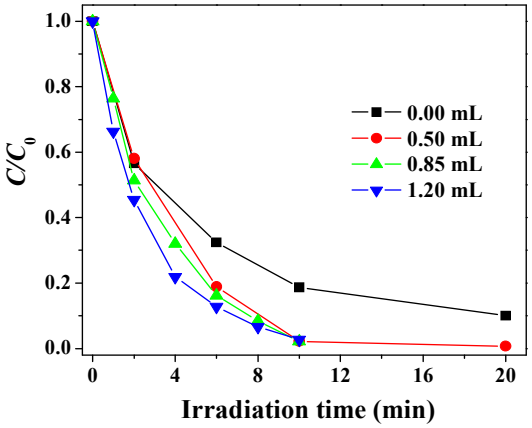

Figure 13. Photocatalytic reduction of aqueous Cr(VI) over CNSS-30 with different amounts of H_2SO_4 solution (1.0 M) added.

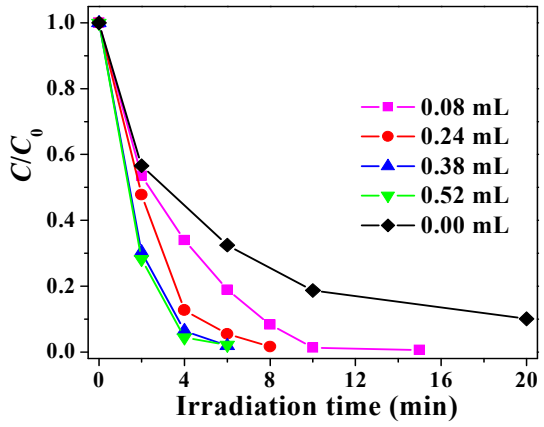

Figure 14. Photocatalytic reduction of aqueous Cr(VI) by CNSS-30 under visible light irradiation with different amounts of HCOOH (hole scavenger) added.

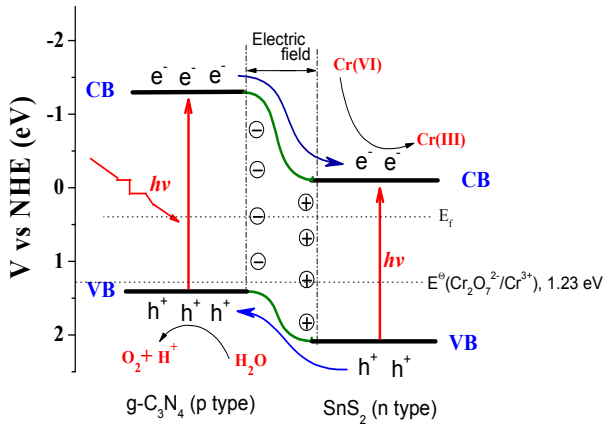

Scheme 1. Photocatalytic reduction mechanism for aqueous Cr(VI) over g-C_3N_4/SnS_2 composites under visible light irradiation.

Conclusions

Novel visible-light induced 3D flower-like g-C_3N_4/SnS_2 composite photocatalyst were successfully synthesized via a facile solvothermal method. The EIS and PC experiments proved that the formation of heterojunction structure between g-C_3N_4 and SnS_2 effectively enhanced the separation efficiency of electrons and holes. The g-C_3N_4/SnS_2 photocatalysts exhibited efficient photocatalytic activities in the reduction of Cr(VI) under visible light, among of which the CNSS-30 revealed the best activity. And about 99% of aqueous Cr(VI) deoxidized within 50 min of reaction in neutral solution. The improved photocatalytic activities of g-C_3N_4/SnS_2 hybrid composites should be ascribed to the high charge separation efficiency and the suitable energy band positions. This study demonstrates that g-C_3N_4 was a very promising candidate for developing visible light-responsive photocatalysts with high photocatalytic activities.

Acknowledgment

This work was financially supported by the NSFC of China (No. 21103069, 21375047, 21175057, 21277059, and 40672158), Scientific Research Reward Fund for Excellent Young and Middle-Aged Scientists of Shandong Province (BS2012HZ001), the Science and Technology Plan Project of Jinan (No. 201307010), and Scientific Research Foundation for Doctors of University of Jinan (XBS1037 and XKY1043).

References

1 M. Yemane, B.S. Chandravanshi and T. Wondimu, *Ethiopia, Food Chem.* 2008, **107**, 1236.
2 L. Khezami and R. Capart, *J. Hazard. Mater.* 2005, **123**, 223.
3 P. Lakshmipathiraj, G.B. Raju, M.R. Basariya, S. Parvathy and S. Prabhakar, *Sep. Purif. Technol.* 2008, **60**, 96.
4 C.J. Lin, S.L. Wang, P.M. Huang, Y.M. Tzou, J.C. Liu, C.C. Chen, J.H. Chen and C. Lin, *Water Res.* 2009, **43**, 5015.
5 A. Olad and R. Nabavi, *J. Hazard. Mater.* 2007, **147**, 845.
6 N. Wang, L.H. Zhu, K.J. Deng, Y.B. She, Y.M. Yu and H.Q. Tang, *Appl. Catal. B: Environ.* 2010, **95**, 400.
7 R. Gherbi, N. Nasrallah, A. Amrane, R. Maachi and M. Trari, *J. Hazard. Mater.* 2011, **186**, 1124.
8 A. Kleiman, A. Márquez, M.L. Vera, J.M. Meichtry and M.I. Litter, *Appl. Catal. B: Environ.* 2011, **101**, 676.
9 S.L. Luo, Y. Xiao, L.X. Yang, C.B. Liu, F. Su, Y. Li, Q.Y. Cai and G.M. Zeng, *Sep. Purif. Technol.* 2011, **79**, 85.
10 L.X. Yang, Y. Xiao, S.H. Liu, Y. Li, Q.Y. Cai, S.L. Luo and G.M. Zeng, *Appl. Catal. B: Environ.* 2010, **94**, 142.
11 X.J. Liu, L.K. Pan, Q.F. Zhao, T. Lv, G. Zhu, T.Q. Chen, T. Lu, Z. Sun and C.Q. Sun, *Chem. Eng. J.* 2012, **183**, 238.
12 H.T. Hsu, S.S. Chen and Y.S. Chen, *Sep. Purif. Technol.* 2011, **80**, 663.
13 J.J. Testa, M.A. Grela and M.I. Litter, *Environ. Sci. Technol.* 2004, **38**, 1589.
14 R. Mu, Z. Xu, L. Li, Y. Shao, H. Wan and S. Zheng, *J. Hazard. Mater.* 2010, **176**, 495.
15 H. Yu, S. Chen, X. Quan, H. Zhao and Y. Zhang, *Environ. Sci. Technol.* 2008, **42**, 3791.
16 L. Lin, Y. Yang, L. Men, X. Wang, D. He, Y. Chai, B. Zhao, S. Ghoshroy, Q. Tang, *Nanoscale,* 2013, **5**, 588.
17 G.D. Chen, M. Sun, Q. Wei, Z. M. Ma and B. Du, *Appl. Catal. B: Environ.* 2012, **125**, 282.
18 Y.C. Zhang, Z.N. Du, K.W. Li, M. Zhang and D.D. Dionysiou, *ACS Appl. Mater. Interfaces* 2011, **3**, 1528.
19 S.D. Zhuang, X.Y. Xu, B. Feng, J.G. Hu, Y.R. Pang, G. Zhou, L. Tong and Y.X. Zhou, *ACS Appl. Mater. Interfaces* 2014, **6**, 613.
20 Y.P. Huang, H. Ma, S.G. Wang, M.W. Shen, R. Guo, X.Y. Cao, M.F. Zhu and X.Y. Shi, *ACS Appl. Mater. Interfaces* 2012, **4**, 3054.
21 Z. Chen and Y.J.Xu, *ACS Appl. Mater. Interfaces* 2013, **5**, 13353.
22 Y.C. Zhang, J. Li, M. Zhang and D.D. Dionysiou, *Environ Sci Technol.* 2011, **45**, 9324.
23 Y.C. Zhang, Z.N. Du, S.Y. Li and M. Zhang, *Appl. Catal. B: Environ.* 2010, **95**, 153.
24 C. Yang, W. Wang, Z. Shan and F. Huang, *J. Solid State Chem.* 2009, **182**, 807.
25 J. Li, X.H. Du, L.Yao, Y.C. Zhang, *Mater. Lett.* 2014, **121**, 44.
26 Y.C. Zhang, J. Li and H.Y. Xu, *Appl. Catal. B: Environ.* 2012, **123-124**, 18.
27 X.C. Wang, K. Maeda, A. Thomas, K. Takanabe, G. Xin, J. M Carlsson, K. Domen and M. Antonietti, *Nat. Mater.* 2009, **8**, 76.
28 X.C. Wang, K. Maeda, X.F. Chen, K. Takanabe, K. Domen, Y.D. Hou, X.Z. Fu and M. Antonietti, *J. Am. Chem. Soc.* 2009, **131**, 1680.
29 K. Takanabe, K. Kamata, X.C. Wang, M. Antonietti, J. Kubota and K. Domen, *Phys. Chem. Chem. Phys.* 2010, **12**, 13020.
30 Q. Xiang, J. Yu and M. Jaroniec, *J. Phys. Chem.* C 2011, **115**, 7355.
31 L. Ge and C. Han, *Appl. Catal. B: Environ.* 2012, **117-118**, 268.
32 L. Ge, C. Han, X. Xiao and L. Guo, *Int. J. Hydrogen Energy* 2013, **38**, 6960.
33 S. Ye, L.G. Qiu, Y.P. Yuan, Y.J. Zhu, J. Xia and J.F. Zhu, *J. Mater. Chem. A* 2013, **1**, 3008.
34 H. Ji, F. Chang, X. Hu, W. Qin and J. Shen, *Chem. Eng. J.* 2013, **218**, 183.
35 S.W. Zhang, J.X. Li, M.Y. Zeng, G.X. Zhao, J.Z. Xu, W.P. Hu and X.K. Wang, *ACS Appl. Mater. Interfaces* 2013, **5**, 12735.
36 Y. Lan, X. Qian, C. Zhao, Z. Zhang, X. Chen and Z. Li, *J. Colloid Interface Sci.* 2013, **395**, 75.
37 X. Guo, G.T.Fei, H. Su and L.D. Zhang, *J. Phys. Chem. C* 2011, **115**, 1608.
38 G. Zhang, J. Zhang, M. Zhang and X. Wang, *J. Mater. Chem.* 2012, **22**, 8083.
39 J. Liu, T. Zhang, Z. Wang, G. Dawson and W. Chen, *J. Mater. Chem.* 2011, **21**, 14398.
40 T.T. Li, L.H. Zhao, Y.M. He, J. Cai, M.F. Luo, J.J. Li, *Appl. Catal. B: Environ.* 2013, **129**, 255.
41 S. Kumar, T. Surendar, A. Baruah and V. Shanker, *J. Mater. Chem. A*, 2013, **1**, 5333.
42 X.J. Bai, L. Wang and Y.F. Zhu, *ACS Catalysis* 2012, **2**, 2769.
43 Y. Ku and I.L. Jung, *Wat. Res.* 2001, **35**, 135.
44 J.M. Joseph, H. Destaillats, H.M. Hung and M.R.Hoffmann, *J. Phys. Chem. A* 2000, **104**, 301.
45 M. Mrowetz and E. Selli, *New J. Chem.* 2006, **30**, 108.
46 M. Mrowetz and E. Selli, *J. Photochem. Photobiol. A: Chem.* 2006, **180**, 15.
47 M. Kaise, H. Nagai, K. Tokuhashi, S. Kondo, S. Nimura and O. Kikuchi, *Langmuir* 1994, **10**, 1345.

48 P. Madhusudan, J.R. Ran, J. Zhang, J.G. Yu and G. Liu, *Appl. Catal. B: Environ.* 2011, **110**, 286.
49 J. Li, T.X. Wang and X.H. Du, *Sep. Purif. Technol.* 2012, **101**, 11.
50 Q.L. Yang, S.Z. Kang, H. Chen, W. Bu and J. Mu, *Desalination* 2011, **266**, 149.
51 S. Tuprakay and W. Liengcharernsit, *J. Hazard. Mater.* 2005, **124**, 53.

Facile fabrication of 3D flower-like heterostructured g-C_3N_4/SnS_2 composite with efficient photocatalytic activity under visible light

Meng Sun,[a] Qing Yan,[a] Tao Yan,[b,c] Mengmeng Li, [b] Dong Wei,[a] Zhongpeng Wang,[a] Qin Wei,[d] and Bin Du [*,a]

[a] School of Resources and Environment, University of Jinan, Shandong Provincial Engineering Technology Research Center for Ecological Carbon Sink and Capture Utilization, Jinan 250022, P.R. China. Fax: +86 531-82765969; Tel: +86 531-82769235; E-mail: binduujn@163.com

[b] School of Civil Engineering and Architecture, University of Jinan, Jinan250022, P.R. China.

[c] School of Chemistry, Beijing Institute of Technology, Beijing 100081, P.R. China.

[d] Key Laboratory of Chemical Sensing & Analysis in Universities of Shandong, School of Chemistry and Chemical Engineering, University of Jinan, Jinan 250022, P.R. China

Graphical abstract

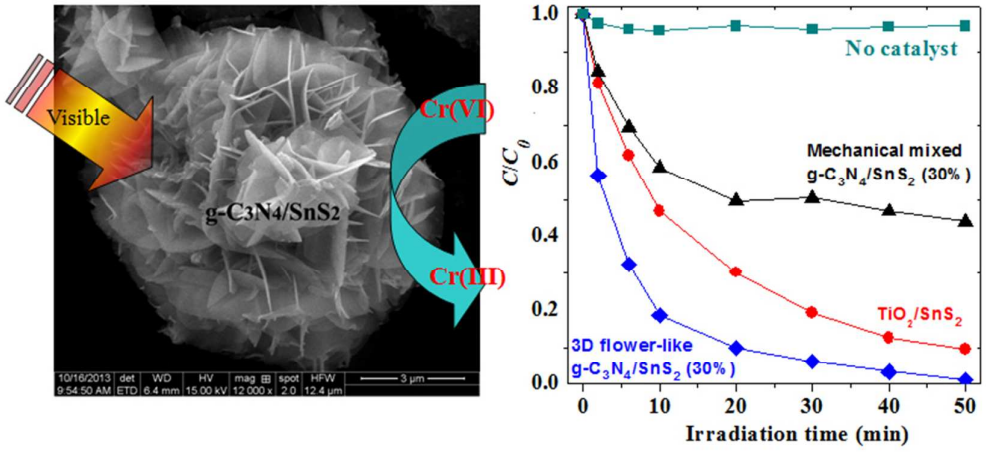

The formation of heterojunction between g-C_3N_4 and SnS_2 greatly enhanced the photocatalytic activity of g-C_3N_4/SnS_2 compared with the mechanical mixed g-C_3N_4/SnS_2.